Theory of electric polarization induced by magnon transport in two-dimensional honeycomb antiferromagnets

D. Quang To,¹ Federico Garcia-Gaitan,² Yafei Ren,² Joshua M. O. Zide,¹ M. Benjamin Jungfleisch,² John Q. Xiao,² Branislav K. Nikolić,² Garnett W. Bryant,³,⁴ and Matthew F. Doty¹,∗

¹Department of Materials Science and Engineering, University of Delaware, Newark, Delaware 19716, USA ²Department of Physics and Astronomy, University of Delaware, Newark, Delaware 19716, USA ³Nanoscale Device Characterization Division, Joint Quantum Institute, National Institute of Standards and Technology, Gaithersburg, Maryland 20899-8423, USA ⁴University of Maryland, College Park, Maryland 20742, USA (Dated: July 24, 2024)

We introduce a quantum mechanical formalism for computing the electric polarization arising in two-dimensional (2D) antiferromagnets (AFMs) as a result of **both** spin and orbital transport effect of magnons. We first show that an applied temperature gradient in a 2D collinear honeycomb AFM gives rise to accumulations of magnons having both orbital moment and spin moment at the edges of the 2D AFM as the manifestation of the magnon Nernst effects. We then use our formalism to show that such magnon Nernst effects, in the presence of the Dzyaloshinskii-Moriya Interaction (DMI), induce electric polarization that can be measured experimentally. Finally, we demonstrate the value of this formalism by using it to predict the properties of two 2D honeycomb AFMs, one each with Néel and zigzag order. These results integrate advances in magnonics, spinorbitronics, and orbitronics to create a unified framework that can be used to understand and control the manipulation of magnetic states in 2D AFMs through the magnon spin and orbital degrees of freedom.

I. INTRODUCTION

Magnons are bosonic quasi-particles arising from collective and charge-neutral excitations of localized spins. These quanta obey the Bose-Einstein distribution function at finite temperatures, possessing a zero chemical potential in equilibrium. Magnons provide an intriguing opportunity for information transmission devoid of energy dissipation because they can propagate over long distances without any charge flow [1–5]. Previous investigations of the thermal transport of magnons have examined their intriguing characteristics through the magnon Seebeck effect (SE) [6], thermal Hall effect (THE) [7–15], and spin Nernst effect (SNE) [16–22]. These effects involve the generation of longitudinal and transverse heat currents or spin currents, mediated by magnons, in response to a longitudinal applied temperature gradient.

In electronic systems, it has been recently recognized that orbital angular moment (OAM) of electrons can generate a number of previously overlooked transport effects [23–30]. Magnon OAM is expected to play a similarly important role in the form of a magnon Orbital Nernst Effect (ONE). Electronic OAM effects are typically considered by analyzing the magnetization and/or electric polarization that results from the orbital motion of the electron charge and spin. While a few studies have very recently explored magnon OAM within different crystalline lattices, [31–37] these studies have focused on theoretical measures of magnon OAM such as

a magnon orbital magnetization [32] or the integral of magnon OAM over the orientation of the magnon wave vector [33, 35]. The absence of a comprehensive theory relating magnon SNE and ONE to experimentally measurable quantities impedes both theoretical and experimental [21] understanding of magnon SNE and ONE, which we collectively refer to as magnon Nernst effects (MNEs).

In this paper we present a quantum mechanical formalism that establishes the connection between magnon transport effects and experimentally measurable quantities, specifically the MNEs and electric polarization, in 2D AFMs on a honeycomb lattice. While the magnon SNE has been extensively studied in the literature [16– 22, the magnon ONE was first introduced in reference [38] using a semiclassical theory. However, reference [38] does not include a clear delineation of the conditions under which semiclassical theory is applicable and, more importantly, does not address the resulting measurable quantities that will be induced by the ONE. The formalism presented here provides a firm quantum mechanical foundation for studying the magnon ONE and its observable manifestation in the form of electric polarization. We note that a recent paper by Neumann, et al discusses the fluctuation-activated electric polarization in chiral edge magnonic system [39]. In this work, we present a formalism that connects the spin current and orbital moment of magnons to the electric polarization. Finally, we note that the authors in Ref. [37] claim that the electric polarization induced by magnon ONE in a honeycomb lattice of a Néel ordered 2D AFM exists even in the absence of the Dzyaloshinskii-Moriya Interaction. According to their claim, this effect only manifests in the

^{*} doty@udel.edu

presence of a finite externally applied magnetic field. Our formalism challenges their prediction.

The paper is structured as follows: In Sect. II we introduce our Hamiltonian model for the 2D honeycomb AFMs. In Sect. III we describe the origin of MNEs in these materials. In Sect. IV we introduce the quantum mechanical formalism that allows for the prediction of experimentally-measurable quantities as a result of the MNEs. In Sect. V we demonstrate the value of this formalism by applying it to examine AFMS with Néel and Zigzag order. We show, using both our formalism and symmetry arguments, that spin orbit coupling in the form of the DMI is necessary to induce measurable electric polarization at the sample edges.

Our work integrates advances in magnonics, spinor-bitronics, and orbitronics within a single unified framework. The results suggest a method for experimental study of magnon OAM and magnon ONE. They also provides an alternative way to probe magnon SNE. More-

over, these results suggest a way to exploit the orbital degree of freedom of magnons in addition to their spin moment, which advances the emerging fields of magnon orbitronics and magnon spinorbitronics and may provide a path to improving high-speed devices based on spin wayes.

II. MODEL AND METHODS

We consider 2D AFM systems on a honeycomb lattice, which can have either Néel or Zigzag ordering as shown in Fig. 1(c) and (d), respectively. In either case, spins lie on A and B sublattices with $S_A = -S_B = S\hat{z}$; the z-axis is out of the plane of the 2D material, as shown in Fig. 1(a). The fundamental spin Hamiltonian for this type of system can be expressed as follows [17, 19, 22]:

$$H = \sum_{i,j} J_{ij} \mathbf{S}_i \cdot \mathbf{S}_j + \Delta \sum_i (S_i^z)^2 + g\mu_B B_z \sum_i S_i^z + \sum_{\langle \langle i,j \rangle \rangle} \mathbf{D}_{ij} \left(\mathbf{S}_i \times \mathbf{S}_j \right)$$
(1)

where $S_i = (S_i^x, S_i^y, S_i^z)$ is the operator of total spin localized at a site i of the lattice. The first term represents the exchange energy, with J_{ij} the exchange coupling between spins localized at sites i and j. The sum \sum_{ij} runs over all atom pairs in the lattice up to the third-nearest neighbor, as shown in Fig. 1b. The second term involves Δ , the easy-axis anisotropy energy. The third term represents the Zeeman energy arising from coupling to the applied magnetic field B_z pointing along the z-axis, which is perpendicular to the plane. Here g is the Landé g-factor and μ_B is the Bohr magneton. Finally, the fourth term captures the Dzyaloshinskii–Moriya Interaction (DMI) with the DMI vector \mathbf{D}_{ij} oriented in the z-direction. The notation $\langle \langle , \rangle \rangle$ indicates a summation over second nearest neighbors.

We employ the Holstein-Primakoff (HP) transformation [40] that maps spin operators residing on sublattice A or B of a 2D AFM to boson operators. The square roots of operators are expanded into a Taylor series and then truncated [41] to linear order to obtain

$$\begin{split} S_A^+ &= \sqrt{2S} a_i, \ S_A^- &= \sqrt{2S} a_i^{\dagger}, \ S_A^z = S - a_i^{\dagger} a_i, \\ S_B^+ &= \sqrt{2S} b_j^{\dagger}, \ S_B^- &= \sqrt{2S} b_j, \ S_B^z = -S + b_j^{\dagger} b_j. \ \ (2) \end{split}$$

The truncation to linear order is valid as long as the temperature is low, $k_BT \ll J_{ij}$ where J_{ij} is the exchange coupling, and the number of magnons excited is sufficiently small [41]. This condition is met when the temperature is much lower than the Néel temperature of an AFM material, of order $T_N = 150~K$ for the 2D AFM materials considered here. We then

recast the spin Hamiltonian as a bosonic Bogoliubov-de Gennes (BdG) Hamiltonian [13] $H = \sum_{\mathbf{k}} \Psi^{\dagger} H(\mathbf{k}) \Psi$ where $\Psi^{\dagger} = [x_{\mathbf{k},1}^{\dagger}, x_{\mathbf{k},2}^{\dagger}, ..., x_{\mathbf{k},n}^{\dagger}, x_{-\mathbf{k},1}, x_{-\mathbf{k},2}, ..., x_{-\mathbf{k},n}]$ is the Nambu spinor. By using Colpa's method [42], we diagonalize this Hamiltonian to obtain the eigenenergies $E_{n,\mathbf{k}}$ and eigenvectors $|n(\mathbf{k})\rangle$ of the system, which is what we use in the following to compute the magnon ONE from linear response theory. Please see the Supplementary Material (SM) [43] for additional information on the construction of the BdG Hamiltonian and the magnetic parameters of the materials employed in this model Hamiltonian.

III. ORIGIN OF MAGNON NERNST EFFECTS

Magnons are inherently charge-neutral entities and cannot be directly manipulated by electric fields. However, magnons can be generated by the introduction of a temperature gradient that induces a transverse magnon thermal current via the THE and a magnon spin current via the SNE. We first show that such thermal gradients can also generate a magnon orbital current (MOC).

In the semiclassical picture, the motion of a magnon wavepacket in the \mathbf{n}^{th} band with position \boldsymbol{r}_c^n and wavevector \boldsymbol{k} subject to an applied temperature gradient obeys [44, 45]: $\dot{\boldsymbol{r}}_c^n = \frac{1}{\hbar} \frac{\partial E_{n,k}}{\partial \boldsymbol{k}} - \dot{\boldsymbol{k}} \times \boldsymbol{\Omega}^n(\boldsymbol{k})$; $\hbar \dot{\boldsymbol{k}} = -\nabla U(\boldsymbol{r})$ where $U(\boldsymbol{r})$ is a slowly varying potential experienced by the magnons; $\boldsymbol{\Omega}^n(\boldsymbol{k}) = \sum_{m \neq n} \boldsymbol{\Omega}^{nm}(\boldsymbol{k})$ is the Berry cur-

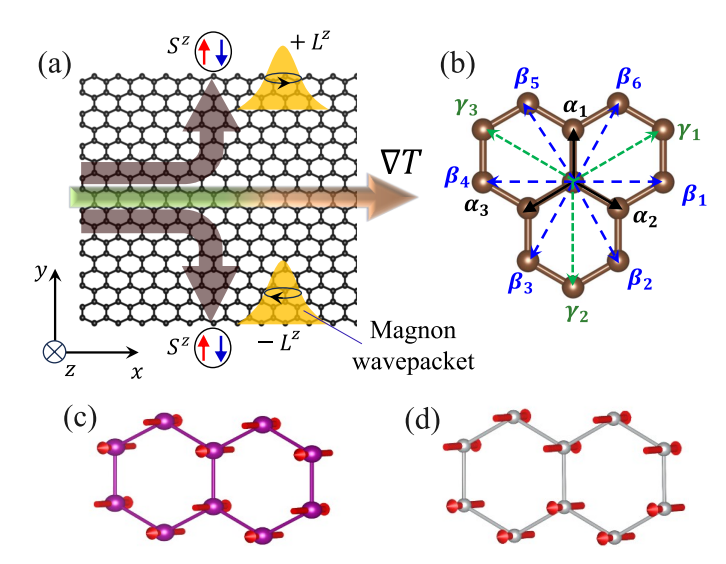


FIG. 1. (a) Schematic view of the magnon ONE in a 2D AFM where transverse flow of magnons carrying opposite out-of-the plane orbital moment is induced by temperature gradient ∇T along the longitudinal direction. (b) The nearest, second nearest and third-nearest neighbor bonds in a honeycomb lattice are denoted by α_i , β_i and γ_i , respectively. (c) Néel and (d) Zigzag ordering of honeycomb spin lattices.

vature with

$$\mathbf{\Omega}^{nm}(\mathbf{k}) = i\hbar^2 \sigma_3^{mm} \sigma_3^{nn} \frac{\langle n(\mathbf{k})|\hat{\mathbf{v}}|m(\mathbf{k})\rangle \times \langle m(\mathbf{k})|\hat{\mathbf{v}}|n(\mathbf{k})\rangle}{(\sigma_3^{nn} E_{n,\mathbf{k}} - \sigma_3^{mm} E_{m,\mathbf{k}})^2}$$
(3)

the projection of the Berry curvature of the \mathbf{n}^{th} band on the \mathbf{m}^{th} band; $E_{n,k}$ and $|n(k)\rangle$ are, respectively, the eigenvectors and eigenvalues of the BdG Hamiltonian; $\hat{\boldsymbol{v}}=(\hat{v}_x,\hat{v}_y,\hat{v}_z)$ denotes the velocity vector operator; and the $\boldsymbol{\sigma}_3$ matrix is given by $\boldsymbol{\sigma}_3=\begin{pmatrix}\mathbf{1}_{N\times N}&0\\0&-\mathbf{1}_{N\times N}\end{pmatrix}$, where $\mathbf{1}_{N\times N}$ is a $N\times N$ identity matrix and $\sigma_3^{nn}=\langle n(k)|\boldsymbol{\sigma}_3|n(k)\rangle$ is the \mathbf{n}^{th} diagonal element of $\boldsymbol{\sigma}_3$.

It is important to note that the Berry curvature plays a pivotal role in generating both the magnon THE and the non-trivial topology of magnon bands [11, 44, 46–49]. The non-trivial topology originates from the motion of magnon wavepackets along the edge of the system [44]. Magnon wavepackets also exhibit self-rotation, referred to as magnon OAM, as elucidated by Matsumoto using linear response theory [44]. As a result, in systems that have both a) non-trivial topological thermal transport of magnons and b) finite self-rotation of magnon wavepackets, the thermal Hall current induced by the magnon bands can also facilitate the transport of magnon OAM. This, in turn, gives rise to a MOC in response to an applied temperature gradient. We call this phenomenon the magnon ONE [Fig. 1(a)]. The consequence of a finite ONE in 2D honeycomb AFMs is the accumulation of the out-of-plane OAM of magnons, L^z , at the boundaries of the system. In this simple picture, the magnon orbital angular moment population accumulated at the edge of the system due to the ONE is directly proportional to

$$\lambda_{xy}^{L^z} = \frac{k_B}{2\hbar V} \sum_{\mathbf{k}} \sum_{n=1}^{N} \sum_{m \neq n} \left\{ \left[\sigma_3^{nn} L_{nn}^z \left(\mathbf{k} \right) + \sigma_3^{mm} L_{mm}^z \left(\mathbf{k} \right) \right] \Omega_{xy}^{nm} \left(\mathbf{k} \right) F(\rho_{n,\mathbf{k}}) \right\}. \tag{4}$$

where $\lambda_{xy}^{L^z}$ is the Orbital Nernst conductivity (ONC); V is the volume of the system; $\rho_{n,\mathbf{k}} = \left(e^{E_{n,\mathbf{k}}/k_BT} - 1\right)^{-1}$ is the Bose-Einstein distribution function; $F\left(\rho_{n,\mathbf{k}}\right) = \left(1 + \rho_{n,\mathbf{k}}\right) \ln\left(1 + \rho_{n,\mathbf{k}}\right) - \rho_{n,\mathbf{k}} \ln\left(\rho_{n,\mathbf{k}}\right)$; $\Omega_{xy}^{nm}\left(\mathbf{k}\right)$ is the out-of-plane component of the projected Berry curvature [Eq. (3)] and L_{nn}^z is the z-component of the intra-band magnon OAM in the Bloch wave of the n^{th} band given by

$$L_{nn}(\mathbf{k}) = -\frac{i\hbar}{2} \sum_{p \neq n} \sigma_3^{pp} \frac{\langle n(\mathbf{k}) | \hat{\mathbf{v}} | p(\mathbf{k}) \rangle \times \langle p(\mathbf{k}) | \hat{\mathbf{v}} | n(\mathbf{k}) \rangle}{\sigma_3^{nn} E_{n,\mathbf{k}} - \sigma_3^{pp} E_{p,\mathbf{k}}}.$$
(5)

For the detailed derivation of these formulas, please refer to the SM [43].

Several physical consequences related to the ONE can be gleaned from Eqs. (4) and (5). (1) The representation

of the magnon intra-band OAM in Bloch states given by Eq. (5) has deep connections to the magnon Berry curvature given in Eq. (3). Specifically, both are subject to the constraints of time reversal symmetry (TRS) and parity-time symmetry (PTS). TRS requires that $L_{nn}(\mathbf{k}) = -L_{nn}(-\mathbf{k})$. PTS requires the intra-band OAM to be zero, as expressed by $L_{nn}(\mathbf{k}) = 0$ [22]. Thus, non-zero intra-band OAM can only be achieved when PTS is broken. (2) Broken TRS is crucial for observing a finite magnon THE. However, Eq. (4) tells us that the ONE can exist even without breaking TRS. The term $\Omega_{xy}^{L^z,nm}(\mathbf{k}) = \frac{1}{4} \left[\sigma_3^{nn} L_{nn}^z(\mathbf{k}) + \sigma_3^{mm} L_{mm}^z(\mathbf{k})\right] \Omega_{xy}^{nm}(\mathbf{k})$ has even parity with respect to the wavevector because both intra-band OAM and Berry curvature have the same parity with respect to the vector \mathbf{k} . As a result, λ_{xy}^{Lz} can be finite even in the presence of TRS. This observation, in combination with point (1) above, suggests that the best

strategy for experimentally observing the ONE is to identify material systems exhibiting finite Berry curvature (i.e. breaking PTS) and thus having nonzero intra-band OAM. Collinear 2D honeycomb AFMs with both Néel and Zigzag phases are promising in this context. (3) Magnon intra-band OAM can have much larger magnitude than magnon spin moment, particularly in the vicinity of the anti-crossing point between two distinct bands. This is similar to the behavior of Berry curvature. Consequently, the ONE should be larger in magnonic crystals in which there are more band crossings for magnons and/or more coupling with other quasiparticles such as phonons [22, 50]. This suggests that the ONE will be more pronounced in systems characterized by strong band hybridization and a narrow energy gap between the bands because the magnitude of both intra-band OAM and Berry curvature are significantly amplified under these conditions [22].

We note that our discussion above illustrates the

ONE using a simple picture in which the topological magnon thermal Hall current gives rise to the magnon ONE through magnon intra-band OAM. However, both magnon intra-band and inter-band OAM can contribute. To treat intra-band and inter-band OAM on an equal footing, we employ the linear response theory to derive the linear thermal response mechanism governing the flow of magnon OAM as

$$j_y^{L^z} = -\lambda_{xy}^{L^z} \partial_x T \tag{6}$$

where

$$\lambda_{xy}^{L^z} = \frac{2k_B}{\hbar V} \sum_{\mathbf{k}} \sum_{n=1}^{N} \Omega_{xy}^{L^z, n} (\mathbf{k}) F(\rho_{n, \mathbf{k}})$$
 (7)

is the total Orbital Nernst conductivity with the total Orbital Berry curvature given by

$$\Omega_{xy}^{L^{z},n}\left(\boldsymbol{k}\right) = -\sum_{m\neq n} 2\hbar^{2}\sigma_{3}^{nn}\sigma_{3}^{mm}Im\left\{\frac{\left\langle n\left(\boldsymbol{k}\right)\left|\hat{j}_{x}^{L^{z}}\right|m\left(\boldsymbol{k}\right)\right\rangle\left\langle m\left(\boldsymbol{k}\right)\left|\hat{v}_{y}\right|n\left(\boldsymbol{k}\right)\right\rangle}{\left[\left(\boldsymbol{\sigma}_{3}E_{\boldsymbol{k}}\right)_{mm}-\left(\boldsymbol{\sigma}_{3}E_{\boldsymbol{k}}\right)_{nn}\right]^{2}}\right\}$$
(8)

where $\hat{\boldsymbol{j}}^{\hat{L}^z} = \hat{L}^z \boldsymbol{\sigma}_3 \hat{\boldsymbol{v}} + \hat{\boldsymbol{v}} \boldsymbol{\sigma}_3 \hat{L}^z$ is the orbital current operator. For the detailed derivation of these formulas, please refer to the SM [43].

IV. MAGNETIZATION AND ELECTRIC POLARIZATION INDUCED BY MAGNON NERNST EFFECTS

Experimental detection of the ONE becomes possible when the accumulation of magnon orbital angular moment can be transformed into a magnetization or electric polarization. This is analogous to the way the OHE for electrons can be measured via spin polarizations induced by OHE via spin orbit coupling [51, 52]. Utilizing perturbation theory, Neumann et al. [32] revealed the dependence of the orbital magnetic moment of magnons on the external magnetic field: $\mu_{n,k}^O = -\sum_{m=1}^N \sum_{\alpha=x,y,z} \frac{\partial E_{n,k}}{\partial \hat{\alpha}_m}$.

 $\frac{\partial \hat{\alpha}_m}{\partial B}$ where B is the applied magnetic field, α is the local spin coordinate system and $E_{n,k}$ is the energy of the magnon in nth state. This dependence is a result of spin orbit coupling (SOC) or SOC-like interactions that couple spins to the lattice (e.g. DMI or magnon-phonon coupling). Consequently, the accumulation of the orbital moment of magnons at the boundaries due to the ONE can manifest as a measurable magnetization in systems featuring DMI, magnon-phonon coupling, or similar interactions.

MNEs may also give rise to a local Electric Polarization (EP) at the boundaries of the system [39]. Applying perturbation theory, we calculate the electric dipole moment contribution to the y-component of the net electric polarization induced by the motion of magnons in 2D honeycomb antiferromagnets under an applied temperature gradient along the x-direction (please refer to the SM [43] for further details). Our result yields:

$$P_{y} = \frac{g\mu_{B}}{\hbar W_{y}c^{2}} \sum_{n,\mathbf{k}} \left[\Omega_{xy}^{S^{z},n}\left(\mathbf{k}\right) k_{B}T \ln\left(e^{-\frac{E_{n,\mathbf{k}}}{k_{B}T}} - 1\right) + 2\hbar\sigma_{3}^{nn} S_{nn}^{z} L_{nn}^{z}\left(\mathbf{k}\right) \rho_{n,\mathbf{k}} \right] = P_{y}^{S} + P_{y}^{O}$$

$$\tag{9}$$

where

$$P_y^S = \frac{g\mu_B}{\hbar W_y c^2} \sum_{n,k} \Omega_{xy}^{S^z,n}(k) k_B T \ln \left(e^{-\frac{E_{n,k}}{k_B T}} - 1 \right)$$
 (10)

$$P_y^O = \frac{g\mu_B}{\hbar W_y c^2} \sum_{n,\mathbf{k}} 2\hbar \sigma_3^{nn} S_{nn}^z L_{nn}^z(\mathbf{k}) \rho_{n,\mathbf{k}}$$
(11)

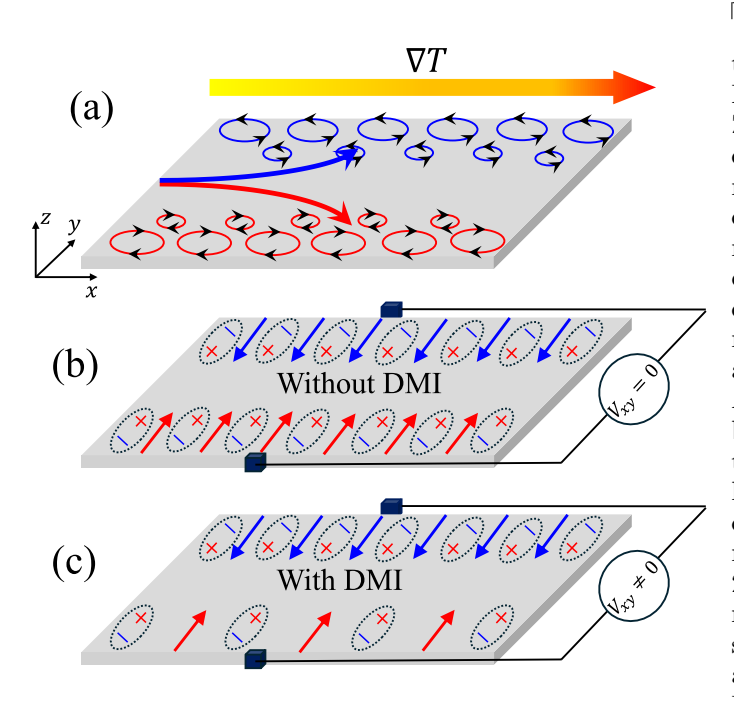


FIG. 2. (a) Schematic illustration of magnon orbital accumulation at the edges of a 2D honeycomb AFM with Néel order under an applied temperature gradient ∇T . (b) The local electric polarization (red and blue arrow) and local polarized charges induced by magnon spin and magnon orbital angular momentum accumulation due to the magnon ONE in the absence of the DMI. The number of charges on each side is equal, resulting in zero net electric polarization in the absence of DMI. (c) The presence of DMI results in a nonzero net polarized charge due to the difference in the populations of magnons carrying opposite OAM.

are the electric polarization induced by magnon spin Berry curvature and magnon orbital angular moment, respectively. Here W_y is the width along the y-direction of the system; k_B is the Boltzmann constant, c is the speed of light in vacuum, T is the temperature, $\Omega_{xy}^{S^z,n}$ is the spin-Berry curvature of nth band, and S_{nn}^z and $L_{nn}^z(k)$ are respectively the spin and OAM of the magnon in the nth band. For a more detailed derivation of this formula, please refer to the SM [43].

Eq. (9) reveals that there are two contributions to the resulting EP: 1) the spin current resulting from the magnon SNE, which is intricately tied to the velocity of the magnon wavepacket's center and 2) the OAM of the magnon, which arises from the inherent self-rotation of the magnon wavepacket. We can now apply our theory

to explain the electric polarization induced by magnon Nernst effects in 2D honeycomb AFMs with Néel and Zigzag order. The presence of a temperature gradient along the x direction leads to the accumulation of magnons with opposite chirality along the $\pm y$ boundaries of the system, as schematically depicted in Fig. 2a. Remarkably, in the absence of DMI the electric polarization completely vanishes for both Néel and Zigzag magnetic orders, even in the presence of an externally applied magnetic field. However, the reasons that EP vanishes in the absence of DMI are different for the two orders. For 2D AFMS in the Zigzag phase, the absence of DMI cause both magnon intra-band OAM and spin Nernst current to vanish (please refer to the SM [43] for details), which leads to zero electric polarization. A finite EP is only observed in the presence of DMI, which induces finite magnon intra-band OAM and spin Nernst current. For 2D AFMs in the Néel order, a finite magnon ONE may result in the accumulation of magnons carrying opposite intra-band OAM at the system's edges even in the absence of DMI while the spin Nersnt current vanishes. However, as shown in Eq. (9), the electric polarization induced by the magnon OAM is governed by the correlation term $S_{nn}^z L_{nn}^z(\mathbf{k})$, which means that for a fixed spin state S_{nn}^z magnons carrying intra-band OAM with opposite signs induce opposite electric polarizations. In other words, the relation $L_{nn}(\mathbf{k}) = -L_{nn}(-\mathbf{k})$ that exists for the Néel order means that the induced local electric polarizations at the edges are opposite in sign but equal in magnitude, resulting in zero total electric polarization across the sample regardless of the externally applied magnetic field, as schematically illustrated in Fig. 2b. A finite total EP is only observed in the case of Néel order when DMI breaks the symmetry between magnons carrying opposite intra-band OAM, as schematically illustrated in Fig. 2c.

We emphasize that the contribution of magnon OAM to electric polarization should not be viewed as a consequence of magnetic dipole moment current circulation. Unlike electrons, which possess charge and whose motion is governed by electric forces, magnons are chargeneutral and their OAM originates solely from the geometrical phase. Therefore, the contributions of magnon OAM to electric polarization should be understood as the changes in the magnon spin current due to the geometrical phase of the magnon wave function, which adds a correction term (P_y^O) to the electric polarization induced by the magnon spin current (P_y^S) as described by Eq. (9),

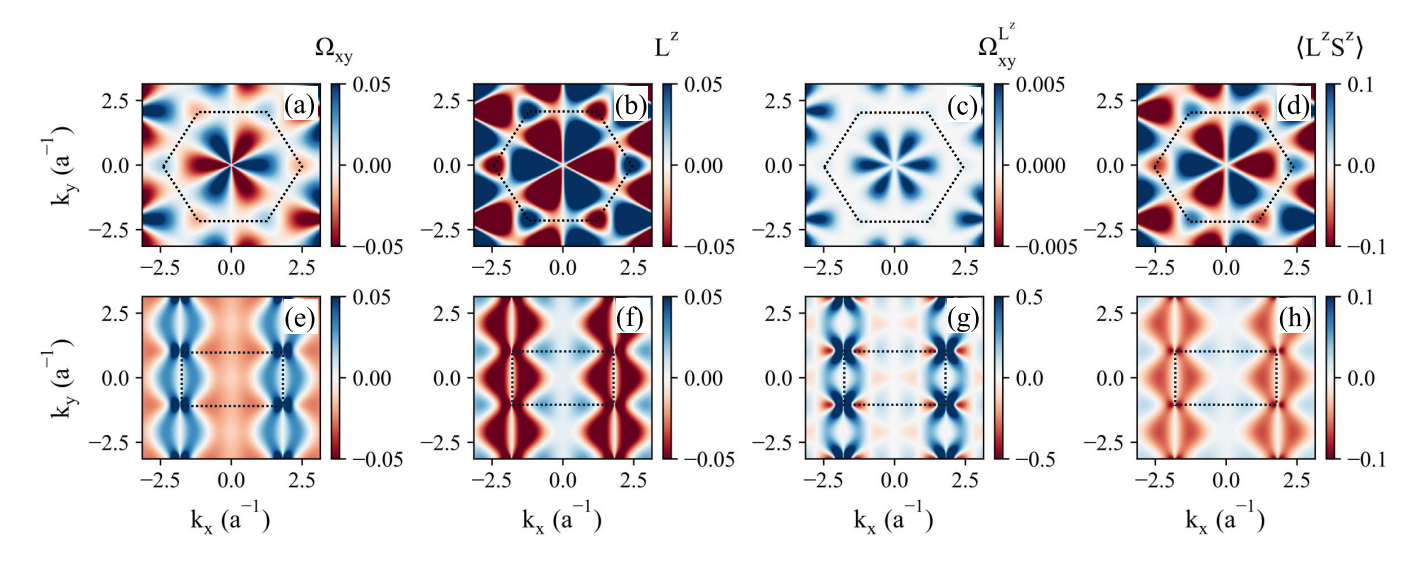


FIG. 3. (a,e) The Berry curvature Ω_{xy} , (b,f) Orbital angular moment L^z in the unit of \hbar , (c,g) Orbital Berry curvature $\Omega_{xy}^{L^z}$, and (d,h) correlation $\langle L^z S^z \rangle$ as a function of the in-plane wavevector (k_x, k_y) . Calculations are performed with applied magnetic field B=1 T for the left-handed magnon mode of MnPS₃ (a-d), which has Néel magnetic order, and NiPSe₃ (e-h), which exhibits Zigzag magnetic order.

which is derived quantum mechanically.

We conclude this section by noting that the electric polarization P_y in Eq. (9) depends on the width W_y of the flake. However, what would be measured in practice is the transverse voltage along the y-direction (V_{xy}) induced by the electric polarization (P_y) under the temperature gradient along x-direction, as shown in Fig. 2(b,c). To derive a prediction of the measurable transverse voltage, we note that the electric field Ξ_y along the y-direction

induced by P_y reads:

$$\Xi_y = \frac{P_y}{\varepsilon_0 \chi} \tag{12}$$

where ε_0 is the electric permittivity of free space and χ is the electric susceptibility. Therefore, the transverse voltage is given by

$$V_{xy} = \int_{0}^{W_y} \Xi_y dy = \frac{g\mu_B}{\hbar \varepsilon_0 \chi c^2} \sum_{n,\mathbf{k}} \left[\Omega_{xy}^{S^z,n} \left(\mathbf{k} \right) k_B T \ln \left(e^{-\frac{E_{n,\mathbf{k}}}{k_B T}} - 1 \right) + 2\hbar \sigma_3^{nn} S_{nn}^z L_{nn}^z \left(\mathbf{k} \right) \rho_{n,\mathbf{k}} \right], \tag{13}$$

which is independent of W_y .

V. MEASURABLE MAGNON NERNST EFFECTS IN REAL MATERIALS

We now apply our formalism to predict the consequences of MNEs in MnPS₃ and NiPSe₃, which are 2D honeycomb AFMs possessing Néel and Zigzag order, respectively. In Fig. 3 we plot the Berry curvature, OAM, orbital Berry curvature (OBC), and the correlation $\langle L^z S^z \rangle^n = S_{nn}^z L_{nn}^z(\mathbf{k})$ as a function of in-plane wavevector (k_x, k_y) for both MnPS₃ (a-e) and NiPS₃ (fj). As expected, these plots display, respectively, the C_3 and C_{2h} symmetries of the magnetic structure in the two. The OBC of both the Néel and Zigzag phases shows the even parity with respect to the wavevector, which may

lead to a finite ONE.

We first consider MnPS₃, which has Néel phase. The correlation function $\langle L^zS^z\rangle^n$ for MnPS₃ exhibits odd parity with respect to the wavevector k, as shown in Fig. 3(d). This occurs because of the odd parity of the magnon intra-band OAM $L_{nn}^z(k)$ even in the presence of DMI, as shown in Fig. 3(b). Without DMI, which is not shown here, this correlation function maintains its odd parity. In the absence of DMI, the system possesses effective time reversal symmetry (TRS) [22], signifying $E_{n,k} = E_{n,-k}$. Consequently, the ONE in the Néel ordered MnPS₃ would not induce any EP without DMI. However, the DMI disrupts this symmetry, leading to $E_{n,k} \neq E_{n,-k}$. This disparity in energy levels results in an imbalance in the population at k and -k, thereby inducing a finite EP, as shown in Fig. 4(c).

In contrast to Néel phase MnPS₃, the correlation func-

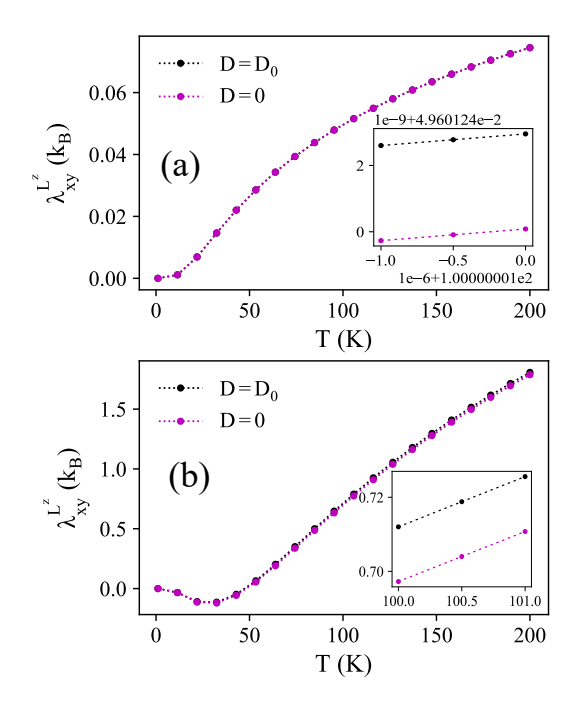


FIG. 4. The ONC of MnPS₃ (a) and NiPSe₃ (b) as a function of temperature at fixed applied magnetic field $B_z=1\ T$. In figures (a) and (b) the black and pink colors indicate the results calculated with and without DMI, respectively, and insets provide a zoomed-in view of the ONC at approximately $T=100\ K$.

tion of NiPSe₃ with Zigzag has even parity with respect to the wavevector in the presence of DMI, as shown in Fig. 3(h). The even parity would induce substantial EP as a result of ONE, as shown in Fig. 4(d). However, in the absence of DMI, the Zigzag phase's correlation function $\langle L^z S^z \rangle^n = S_{nn}^z L_{nn}^z(\mathbf{k})$ vanishes because of vanishing magnon intra-band OAM $L_{nn}^z(\mathbf{k})$, as discussed earlier, resulting in zero contribution to EP. Nonzero EP is only observed when DMI induces finite magnon intraband OAM. In short, DMI plays a pivotal role in enabling the observation of finite contributions of the ONE to EP in both the Néel and Zigzag phases of 2D honeycomb AFMs.

To illustrate the magnitude of the predicted measurable quantities, in Fig. 4 we plot the ONC $\lambda_{xy}^{L_z}$ (a,b) and electric polarization P_y (c,d) of MnPS₃ (a,c) and NiPS₃ (b,d) as a function of temperature T with (black) and without (pink) DMI. Perhaps most importantly, we find that the ONC are about three orders of magnitude larger than the spin Nernst conductivities in the same systems. For instance, the spin Nernst conductivity of NiPSe₃ is about 10^{-3} k_B [20]) and the ONC is predicted to be in the order of k_B. This striking contrast originates in the fact that the magnon spin angular moment in the systems we consider can only have one of two values: The z-component of spin is locked to the magnon chirality and is independent of the wavevector k [16]. In contrast, there is no limit on the maximum OAM of a magnon. Strikingly,

and as shown in Fig. 4(a) and (b), the ONC exists even in the absence of DMI, which indicates that the ONE does not require spin orbit coupling akin to the OHE predicted for electronic systems [23, 53, 54]. This stands in stark contrast to the SNE, where DMI is required to observe non-zero SNE [16]. This disparity arises from the invariance of the systems under the combined $\mathcal{C}_S \mathcal{M}_x \mathcal{T}_a$ symmetry, where \mathcal{C}_S is the spin rotation symmetry operation which flips all the spins (and magnetic fields) in the system, \mathcal{M}_x represents mirror symmetry with respect to the plane perpendicular to the x-axis, and \mathcal{T}_a denotes the translation operator responsible for displacing the system by the vector β_1 or β_4 [see Fig. 1(b)]. The ONE does not require the breaking of $C_S \mathcal{M}_x \mathcal{T}_a$ symmetry, primarily because the OAM is not preserved under non-commutative rotation and translation operations. Consequently, the ONC has non-zero values whether or not DMI is present to break $C_S \mathcal{M}_x \mathcal{T}_a$ symmetry, as illustrated in Figure 4(a) and (b). However, when the $C_S \mathcal{M}_x \mathcal{T}_a$ symmetry is preserved, the spin polarized current along y-direction $j_y^{S^z}$ must vanish [see (SM) [43] for further detail]. In other words, regardless of the externally applied magnetic field, magnon ONE does not induce a spin-polarized current in the absence of DMI. Only when the presence of DMI breaks the $C_S \mathcal{M}_x \mathcal{T}_a$ symmetry does a finite spin current emerge within the system as a result of the SNE. The finite SNE in the presence of DMI coupled with finite ONE results in the observable EP as shown in Figure 5(a) and (b). Meanwhile, as expected, the EP vanishes when DMI is turned off.

Figure 5 illustrates the electric polarization behavior of MnPS₃ [Fig. 5(a)] and NiPSe₃ [Fig. 5(b)] across a range of Dzyaloshinskii-Moriya interaction strengths, denoted by the ratio D/D_0 . The results reveal a notable linear correlation. Remarkably, in the absence of DMI, the electric polarization completely vanishes for both Néel and Zigzag magnetic orders even in the presence of an externally applied magnetic field $B_z = 1 T$. This behavior can be also understood from a symmetry perspective as follows: In the absence of the Dzyaloshinskii-Moriya interaction and externally applied magnetic field, the system maintains mirror symmetry for Néel order \mathcal{M}_{ν} and glide mirror symmetry $\mathcal{M}_y \tau$ for Zigzag order about the plane normal to the y-direction. This results in zero electric polarization along the y-direction because the electric polarization along the y-direction is odd under \mathcal{M}_y or $\mathcal{M}_y \tau$ operation. Since the system holds mirror symmetry \mathcal{M}_y for Néel order and glide mirror symmetry $\mathcal{M}_y \tau$ for Zigzag order, it follows that $P_y \equiv -P_y$ meaning P_y must vanish. The presence of an externally applied magnetic field breaks the mirror symmetry \mathcal{M}_{y} in Néel order and glide mirror symmetry $\mathcal{M}_{y}\tau$ in Zigzag order. However, the magnetic field does not induce any coupling between different magnon bands, resulting in unchanged wavefunctions. Furthermore the relation $E_{n,k} = E_{n,-k}$ is maintained leaving P_y vanished even with the presence of the externally applied magnetic field with the lack of the DMI $(D/D_0 = 0)$ as shown in Fig. 5(a,b). In con-

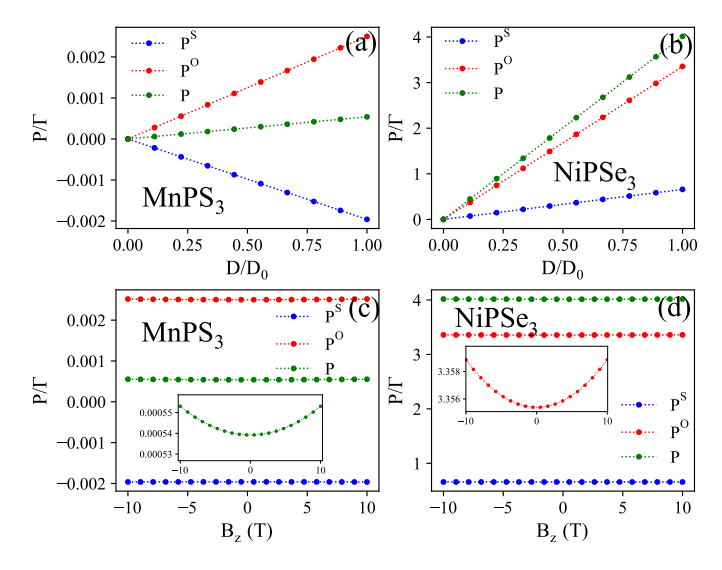


FIG. 5. The electric polarization of MnPS₃ (Figure a) and NiPSe₃ (Figure b) varies as a function of the Dzyaloshinskii-Moriya interaction strength, parameterized by the ratio D/D_0 . Here D_0 represents the baseline DMI strength for each material; $\Gamma = \frac{g\mu_B}{\hbar W_y c^2}$. These calculations were conducted under a constant applied magnetic field of $B_z = 1~T$ and temperature of 100 K. The electric polarization of MnPS₃ (a) and NiPSe₃ (b) varies as a function of the externally applied magnetic field B_z . The insets in both figure a and b zoom in on the total electric polarization to reveal a weak dependence on B_z . These calculations were conducted for a temperature of 100 K.

trast, the presence of DMI breaks the \mathcal{M}_y symmetry and yields to $E_{n,k} \neq E_{n,-k}$ [55, 56], thereby allowing for a finite P_y as observed in Fig. 5(a,b).

In Fig. 5(c,d) we present the dependence of the electric polarization on B_z , the magnetic field externally applied along the z-direction. The total electric polarization P_y , along with its constituents from spin current P_y^S and orbital angular moment P_y^O , exhibit relatively small variations as a function of the magnetic field. This minimal impact results from the magnetic field causing a splitting in the magnon bands corresponding to opposite spins, without inducing any coupling between these distinct bands. Consequently, the weak response of the ONC to the magnetic field B_z arises solely from changes in the magnon population $\rho_{n,k}$ and the function $\left(e^{-\frac{E_{n,k}}{k_BT}}-1\right)$ in Eq. (9), which are due to the shift in the magnon energy band caused by the Zeeman interaction between local spins and external applied magnetic field. Crucially, all components remain finite even at zero magnetic field, suggesting the potential feasibility of detecting the magnon Orbital Nernst effect even in the

We conclude this section with three notes about the possibility of observing the predicted effects in realistic materials. First, we note that the electric polarization in MnPS₃ is approximately three orders of magnitude

absence of an external magnetic field.

smaller than that in NiPSe₃. Additionally, the EP in NiPSe₃ is predominantly influenced by magnon orbital angular moment, whereas in MnPS₃ both the spin Berry curvature and magnon OAM contribute equally to the EP. This indicates that the measurement of EP in the Zigzag order of NiPSe₃ would provide direct evidence of magnon OAM and orbital Nernst effect in this material. Second, in the system considered here the DMI is oriented along the z axis (out of plane), which means it cannot introduce scattering between magnons. In Sect. S6 of the SI we consider what would happen in materials for which this is not the case. Finally, we note that the interaction between magnons and phonons in collinear 2D antiferromagnets and the inherent structure of noncollinear AFMs can break symmetries in a manner similar to the Dzyaloshinskii-Moriya interaction. These effects may also lead to a finite contribution from magnon ONE to the EP in these material systems.

VI. CONCLUSION AND OUTLOOK

In summary, we present a formalism that allows us to connect measurable quantities, namely electric polarization, to magnon spin and orbital moment transport. We introduce the representation of magnon OAM within the Bloch wavefunction, establishing a profound connection between magnon intra-band OAM and magnon Berry curvature. Additionally, we present a full quantum mechanical derivation of electric polarization induced by magnon OAM and magnon spin current. We then apply our formalism to novel phenomena—the Magnon Orbital Nernst Effect and Magnon Spin Nernst Effect—in 2D AFMs exhibiting either Zigzag or Néel order on the honeycomb lattice. Through this approach, we demonstrate that materials with Néel order and/or Zigzag order in a combination with the DMI can generate the electric polarization at the edges of the system as a result of magnon Nernst effects. These intriguing findings point the way toward experimental validation of the predicted magnon SNE and magnon ONE phenomenon in 2D honeycomb AFMs with Néel and Zigzag order (e.g. MnPS₃ and NiPSe₃). They may also catalyze further exploration of the emerging field of magnon orbitronics and magnon spinorbitronics. Finally, it is important to highlight that, although our work focuses on generating MNEs through thermal effects, our findings extend beyond this scope. Our results also indicate that, despite being electrically neutral, magnons can interact with electromagnetic waves via the electric field component of light. Our theory shows that both the spin and orbital moments of magnons contribute to their electric activity. Consequently, we anticipate that light can transfer its angular momentum into the spin and orbital angular momentum of magnons. This insight paves the way for future research on light-driven magnon dynamics in magnetic materials, leveraging the spin and orbital angular momentum degrees of freedom of magnons.

ACKNOWLEDGMENTS

This research was primarily supported by NSF through the University of Delaware Materials Research Science and Engineering Center, DMR-2011824.

- Y. Kajiwara, K. Harii, S. Takahashi, J.-i. Ohe, K. Uchida, M. Mizuguchi, H. Umezawa, H. Kawai, K. Ando, K. Takanashi, et al., Transmission of electrical signals by spin-wave interconversion in a magnetic insulator, Nature 464, 262 (2010).
- [2] A. V. Chumak, V. I. Vasyuchka, A. A. Serga, and B. Hillebrands, Magnon spintronics, Nature physics 11, 453 (2015).
- [3] R. Lebrun, A. Ross, S. Bender, A. Qaiumzadeh, L. Baldrati, J. Cramer, A. Brataas, R. Duine, and M. Kläui, Tunable long-distance spin transport in a crystalline antiferromagnetic iron oxide, Nature 561, 222 (2018).
- [4] W. Xing, L. Qiu, X. Wang, Y. Yao, Y. Ma, R. Cai, S. Jia, X. C. Xie, and W. Han, Magnon transport in quasi-twodimensional Van der Waals antiferromagnets, Phys. Rev. X 9, 011026 (2019).
- [5] P. Pirro, V. I. Vasyuchka, A. A. Serga, and B. Hillebrands, Advances in coherent magnonics, Nature Reviews Materials 6, 1114 (2021).
- [6] J. Xiao, G. E. W. Bauer, K.-c. Uchida, E. Saitoh, and S. Maekawa, Theory of magnon-driven spin Seebeck effect, Phys. Rev. B 81, 214418 (2010).
- [7] Y. Onose, T. Ideue, H. Katsura, Y. Shiomi, N. Nagaosa, and Y. Tokura, Observation of the magnon Hall effect, Science 329, 297 (2010).
- [8] H. Katsura, N. Nagaosa, and P. A. Lee, Theory of the thermal Hall effect in quantum magnets, Phys. Rev. Lett. 104, 066403 (2010).
- [9] R. Matsumoto, R. Shindou, and S. Murakami, Thermal Hall effect of magnons in magnets with dipolar interaction, Phys. Rev. B 89, 054420 (2014).
- [10] M. Hirschberger, R. Chisnell, Y. S. Lee, and N. P. Ong, Thermal Hall effect of spin excitations in a Kagome magnet, Phys. Rev. Lett. 115, 106603 (2015).
- [11] S. Murakami and A. Okamoto, Thermal Hall effect of magnons, Journal of the Physical Society of Japan 86, 011010 (2017).
- [12] X. Zhang, Y. Zhang, S. Okamoto, and D. Xiao, Thermal Hall effect induced by magnon-phonon interactions, Phys. Rev. Lett. 123, 167202 (2019).
- [13] S. Park, N. Nagaosa, and B.-J. Yang, Thermal Hall effect, spin nernst effect, and spin density induced by a thermal gradient in collinear ferrimagnets from magnon-phonon interaction, Nano letters 20, 2741 (2020).
- [14] R. R. Neumann, A. Mook, J. Henk, and I. Mertig, Thermal Hall effect of magnons in collinear antiferromagnetic insulators: Signatures of magnetic and topological phase transitions, Phys. Rev. Lett. 128, 117201 (2022).
- [15] J. N. Kløgetvedt and A. Qaiumzadeh, Tunable topological magnon-polaron states and intrinsic anomalous hall phenomena in two-dimensional ferromagnetic insulators, Phys. Rev. B 108, 224424 (2023).
- [16] R. Cheng, S. Okamoto, and D. Xiao, Spin Nernst effect of magnons in collinear antiferromagnets, Phys. Rev. Lett.

- **117**, 217202 (2016).
- [17] V. A. Zyuzin and A. A. Kovalev, Magnon spin Nernst effect in antiferromagnets, Phys. Rev. Lett. 117, 217203 (2016).
- [18] B. Li, S. Sandhoefner, and A. A. Kovalev, Intrinsic spin Nernst effect of magnons in a noncollinear antiferromagnet, Phys. Rev. Res. 2, 013079 (2020).
- [19] N. Bazazzadeh, M. Hamdi, S. Park, A. Khavasi, S. M. Mohseni, and A. Sadeghi, Magnetoelastic coupling enabled tunability of magnon spin current generation in two-dimensional antiferromagnets, Phys. Rev. B 104, L180402 (2021).
- [20] N. Bazazzadeh, M. Hamdi, F. Haddadi, A. Khavasi, A. Sadeghi, and S. M. Mohseni, Symmetry enhanced spin-nernst effect in honeycomb antiferromagnetic transition metal trichalcogenide monolayers, Phys. Rev. B 103, 014425 (2021).
- [21] H. Zhang and R. Cheng, A perspective on magnon spin Nernst effect in antiferromagnets, Applied Physics Letters 120, 10.1063/5.0084359 (2022).
- [22] D.-Q. To, C. Y. Ameyaw, A. Suresh, S. Bhatt, M. J. H. Ku, M. B. Jungfleisch, J. Q. Xiao, J. M. O. Zide, B. K. Nikolić, and M. F. Doty, Giant spin nernst effect in a two-dimensional antiferromagnet due to magnetoelastic coupling induced gaps and interband transitions between magnonlike bands, Phys. Rev. B 108, 085435 (2023).
- [23] D. Go, D. Jo, C. Kim, and H.-W. Lee, Intrinsic spin and Orbital Hall effects from orbital texture, Phys. Rev. Lett. 121, 086602 (2018).
- [24] D. Go and H.-W. Lee, Orbital torque: Torque generation by orbital current injection, Phys. Rev. Res. 2, 013177 (2020).
- [25] D. Go, F. Freimuth, J.-P. Hanke, F. Xue, O. Gomonay, K.-J. Lee, S. Blügel, P. M. Haney, H.-W. Lee, and Y. Mokrousov, Theory of current-induced angular momentum transfer dynamics in spin-orbit coupled systems, Phys. Rev. Res. 2, 033401 (2020).
- [26] D. Go, D. Jo, K.-W. Kim, S. Lee, M.-G. Kang, B.-G. Park, S. Blügel, H.-W. Lee, and Y. Mokrousov, Longrange orbital torque by momentum-space hotspots, Phys. Rev. Lett. 130, 246701 (2023).
- [27] Y.-G. Choi, D. Jo, K.-H. Ko, D. Go, K.-H. Kim, H. G. Park, C. Kim, B.-C. Min, G.-M. Choi, and H.-W. Lee, Observation of the orbital Hall effect in a light metal Ti, Nature 619, 52 (2023).
- [28] I. Lyalin, S. Alikhah, M. Berritta, P. M. Oppeneer, and R. K. Kawakami, Magneto-optical detection of the Orbital Hall Effect in Chromium, Phys. Rev. Lett. 131, 156702 (2023).
- [29] T. S. Seifert, D. Go, H. Hayashi, R. Rouzegar, F. Freimuth, K. Ando, Y. Mokrousov, and T. Kampfrath, Time-domain observation of ballistic orbital-angularmomentum currents with giant relaxation length in tungsten, Nature Nanotechnology 18, 1132 (2023).

- [30] M. B. Jungfleisch, Observation of ultrafast ballistic orbital transport, Nature Nanotechnology, 1 (2023).
- [31] C. Jia, D. Ma, A. F. Schäffer, and J. Berakdar, Twisted magnon beams carrying orbital angular momentum, Nature Communications 10, 2077 (2019).
- [32] R. R. Neumann, A. Mook, J. Henk, and I. Mertig, Orbital magnetic moment of magnons, Phys. Rev. Lett. 125, 117209 (2020).
- [33] R. S. Fishman, J. S. Gardner, and S. Okamoto, Orbital angular momentum of magnons in collinear magnets, Phys. Rev. Lett. 129, 167202 (2022).
- [34] R. S. Fishman, L. Lindsay, and S. Okamoto, Exact results for the orbital angular momentum of magnons on honeycomb lattices, Journal of Physics: Condensed Matter 51, 015801 (2022).
- [35] R. S. Fishman, Gauge-invariant measure of the magnon orbital angular momentum, Phys. Rev. B 107, 214434 (2023).
- [36] R. S. Fishman, T. Berlijn, J. Villanova, and L. Lindsay, Magnon orbital angular momentum of ferromagnetic honeycomb and zig-zag lattices, arXiv preprint arXiv:2308.16832 10.48550/arXiv.2308.16832 (2023).
- [37] G. Go, D. An, H.-W. Lee, and S. K. Kim, Magnon orbital nernst effect in honeycomb antiferromagnets without spin-orbit coupling, Nano Letters 24, 5968 (2024).
- [38] L.-C. Zhang, F. R. Lux, J.-P. Hanke, P. M. Buhl, S. Grytsiuk, S. Blügel, and Y. Mokrousov, Orbital Nernst effect of magnons, arXiv preprint arXiv:1910.03317 10.48550/arXiv.1910.03317 (2019).
- [39] R. R. Neumann, J. Henk, I. Mertig, and A. Mook, Electrical activity of topological chiral edge magnons, Phys. Rev. B 109, L180412 (2024).
- [40] T. Holstein and H. Primakoff, Field dependence of the intrinsic domain magnetization of a ferromagnet, Phys. Rev. 58, 1098 (1940).
- [41] U. Bajpai, A. Suresh, and B. K. Nikolić, Quantum manybody states and Green's functions of nonequilibrium electron-magnon systems: Localized spin operators versus their mapping to Holstein-Primakoff bosons, Phys. Rev. B 104, 184425 (2021).
- [42] J. Colpa, Diagonalization of the quadratic boson hamiltonian, Physica A: Statistical Mechanics and its Applications 93, 327 (1978).
- [43] See Supplemental Material at https://mrsec.udel.edu/about-ud-charm/ which includes Refs. [57? -74] along with (1) The BdG Hamiltonian of 2D AFM with Néel and Zigzag order (2) Derivations of Eqs. (4), (5), (9).
- [44] R. Matsumoto and S. Murakami, Theoretical prediction of a rotating magnon wave packet in ferromagnets, Phys. Rev. Lett. 106, 197202 (2011).
- [45] D. Xiao, M.-C. Chang, and Q. Niu, Berry phase effects on electronic properties, Rev. Mod. Phys. 82, 1959 (2010).
- [46] G. Go, S. K. Kim, and K.-J. Lee, Topological magnonphonon hybrid excitations in two-dimensional ferromagnets with tunable Chern numbers, Phys. Rev. Lett. 123, 237207 (2019).
- [47] S. Zhang, G. Go, K.-J. Lee, and S. K. Kim, Su(3) topology of magnon-phonon hybridization in 2d antiferromagnets, Phys. Rev. Lett. 124, 147204 (2020).
- [48] S. A. Díaz, J. Klinovaja, and D. Loss, Topological magnons and edge states in antiferromagnetic Skyrmion crystals, Phys. Rev. Lett. 122, 187203 (2019).
- [49] E. Viñas Boström, T. S. Parvini, J. W. McIver, A. Rubio, S. V. Kusminskiy, and M. A. Sentef, Direct optical

- probe of magnon topology in two-dimensional quantum magnets, Phys. Rev. Lett. **130**, 026701 (2023).
- [50] S. Liu, A. Granados del Águila, D. Bhowmick, C. K. Gan, T. Thu Ha Do, M. A. Prosnikov, D. Sedmidubský, Z. Sofer, P. C. M. Christianen, P. Sengupta, and Q. Xiong, Direct observation of magnon-phonon strong coupling in two-dimensional antiferromagnet at high magnetic fields, Phys. Rev. Lett. 127, 097401 (2021).
- [51] S. Ding, A. Ross, D. Go, L. Baldrati, Z. Ren, F. Freimuth, S. Becker, F. Kammerbauer, J. Yang, G. Jakob, Y. Mokrousov, and M. Kläui, Harnessing orbital-to-spin conversion of interfacial orbital currents for efficient spinorbit torques, Phys. Rev. Lett. 125, 177201 (2020).
- [52] T. Li, L. Liu, X. Li, X. Zhao, H. An, and K. Ando, Giant orbital-to-spin conversion for efficient current-induced magnetization switching of ferrimagnetic insulator, Nano Letters 23, 7174 (2023).
- [53] B. A. Bernevig, T. L. Hughes, and S.-C. Zhang, Orbitronics: The intrinsic orbital current in p-doped silicon, Phys. Rev. Lett. 95, 066601 (2005).
- [54] D. Go, D. Jo, H.-W. Lee, M. Kläui, and Y. Mokrousov, Orbitronics: Orbital currents in solids, Europhysics Letters 135, 37001 (2021).
- [55] K. H. Lee, S. B. Chung, K. Park, and J.-G. Park, Magnonic quantum spin hall state in the zigzag and stripe phases of the antiferromagnetic honeycomb lattice, Phys. Rev. B 97, 180401 (2018).
- [56] D. Ghader and A. Khater, A new class of nonreciprocal spin waves on the edges of 2d antiferromagnetic honeycomb nanoribbons, Scientific Reports 9, 15220 (2019).
- [57] R. Kubo, Statistical-mechanical theory of irreversible processes. i. general theory and simple applications to magnetic and conduction problems, Journal of the physical society of Japan 12, 570 (1957).
- [58] R. Kubo, M. Yokota, and S. Nakajima, Statistical-mechanical theory of irreversible processes. ii. response to thermal disturbance, Journal of the Physical Society of Japan 12, 1203 (1957).
- [59] G. D. Mahan, Many-particle physics (Springer Science & Business Media, 2013).
- [60] L. Smrcka and P. Streda, Transport coefficients in strong magnetic fields, Journal of Physics C: Solid State Physics 10, 2153 (1977).
- [61] A. Mook, B. Göbel, J. Henk, and I. Mertig, Taking an electron-magnon duality shortcut from electron to magnon transport, Phys. Rev. B 97, 140401 (2018).
- [62] J. Shi, G. Vignale, D. Xiao, and Q. Niu, Quantum theory of orbital magnetization and its generalization to interacting systems, Phys. Rev. Lett. 99, 197202 (2007).
- [63] D. Xiao, J. Shi, and Q. Niu, Berry phase correction to electron density of states in solids, Phys. Rev. Lett. 95, 137204 (2005).
- [64] T. Thonhauser, D. Ceresoli, D. Vanderbilt, and R. Resta, Orbital magnetization in periodic insulators, Phys. Rev. Lett. 95, 137205 (2005).
- [65] M. Fishman, S. R. White, and E. M. Stoudenmire, The ITensor software library for tensor network calculations, SciPost Phys. Codebases, 4 (2022).
- [66] F. D. M. Haldane, Model for a quantum hall effect without landau levels: Condensed-matter realization of the "parity anomaly", Phys. Rev. Lett. 61, 2015 (1988).
- [67] A. L. Chernyshev and P. A. Maksimov, Damped topological magnons in the kagome-lattice ferromagnets, Phys.

- Rev. Lett. 117, 187203 (2016).
- [68] J. Habel, A. Mook, J. Willsher, and J. Knolle, Breakdown of chiral edge modes in topological magnon insulators, Phys. Rev. B 109, 024441 (2024).
- [69] M. E. Zhitomirsky and A. L. Chernyshev, Colloquium: Spontaneous magnon decays, Rev. Mod. Phys. 85, 219 (2013).
- [70] M. Gohlke, A. Corticelli, R. Moessner, P. A. McClarty, and A. Mook, Spurious symmetry enhancement in linear spin wave theory and interaction-induced topology in magnons, Phys. Rev. Lett. 131, 186702 (2023).
- [71] R. Hoyer, R. Jaeschke-Ubiergo, K.-H. Ahn, L. Šmejkal, and A. Mook, Spontaneous crystal thermal hall effect in

- insulating altermagnets (2024), arXiv:2405.05090 [cond-mat.mes-hall].
- [72] S. R. White and A. E. Feiguin, Real-time evolution using the density matrix renormalization group, Phys. Rev. Lett. 93, 076401 (2004).
- [73] J. Haegeman, C. Lubich, I. Oseledets, B. Vandereycken, and F. Verstraete, Unifying time evolution and optimization with matrix product states, Phys. Rev. B 94, 165116 (2016).
- [74] T. Chanda, P. Sierant, and J. Zakrzewski, Time dynamics with matrix product states: Many-body localization transition of large systems revisited, Phys. Rev. B 101, 035148 (2020).